Rare Met. (2023) 42(1):234–243
https://doi.org/10.1007/s12598-022-02117-8

RARE METALS

ORIGINAL ARTICLE

Timescales and contribution of heating and helicity effect in helicity-dependent all-optical switching

Guan-Qi Li, Xiang-Yu Zheng, Jun-Lin Wang, Xian-Yang Lu, Jing Wu*, Jian-Wang Cai*, Hao Meng, Bo Liu, Thomas A. Ostler, Yong-Bing Xu*

Received: 28 December 2021 / Revised: 12 April 2022 / Accepted: 15 April 2022 / Published online: 22 October 2022

Abstract The heating and helicity effects induced by circularly polarized laser excitation are entangled in the helicity-dependent all-optical switching (HD-AOS), which hinders understanding the magnetization dynamics involved. Here, applying a dual-pump laser excitation, first with a linearly polarized (LP) laser pulse followed by a circularly polarized (CP) laser pulse, the timescales and contribution from heating and helicity effects in HD-AOS were identified with a Pt/Co/Pt triple-layer. When the LP laser pulses preheat the sample to a nearly fully demagnetized state, the CP laser pulses with a power reduced by 80% switch the sample's magnetization. By varying the time delay between the two pump pulses, the results show that the helicity effect, which gives rise to the deterministic helicity-induced switching, arises almost instantly within 200 fs close to the pulse width upon laser excitation. The results reveal that the transient magnetization state upon which CP laser pulses impinge is the key factor for achieving HD-AOS, and importantly, the tunability between heating and helicity effects with the unique dual-pump laser excitation approach will enable HD-AOS in a wide range of magnetic material systems having wide-ranging implications for potential ultrafast spintronics applications.

Keywords Helicity-dependent all-optical switching; Ultrafast laser; Ultrafast magnetization; Magneto-optical interaction

Supplementary Information The online version contains supplementary material available at https://doi.org/10.1007/s12598-022-02117-8.

Guan-Qi Li, Xiang-Yu Zheng and Jun-Lin Wang contributed equally to this work.

G.-Q. Li, J.-L. Wang, J. Wu*
School of Integrated Circuits, Guangdong University of Technology, Guangzhou 510006, China
e-mail: jing.wu@york.ac.uk

G.-Q. Li, X.-Y. Zheng, X.-Y. Lu, J. Wu, Y.-B. Xu
York-Nanjing International Joint Center in Spintronics, School of Electronic Science and Engineering, Nanjing University, Nanjing 210093, China

X.-Y. Zheng, J.-L. Wang, Y.-B. Xu
Spintronics and Nanodevice Laboratory, Department of Electronics Engineering, University of York, York YO10 5DD, UK

J.-W. Cai
Institute of Physics, Chinese Academy of Sciences, Beijing 100190, China

H. Meng, B. Liu
Key Laboratory of Spintronics Materials, Devices and System of Zhejiang Province, Hangzhou 311305, China

T. A. Ostler
College of Business, Technology and Engineering, Sheffield Hallam University, Sheffield S1 1WB, UK

1 Introduction

All-optical magnetization switching (AOS) was first observed in landmark experiment [1], demonstrating that magnetization can be reversed by laser pulses without any applied magnetic field in GdFeCo. The microscopic mechanism for the AOS process in GdFeCo has been considered a helicity-independent heating effect because the Fe and Gd sublattices demagnetize on very different timescales [2]. This leads to a transient ferromagnetic-like state discovered in GdFeCo, which mediates the helicity-

independent all-optical switching (HID-AOS) [3]. HID-AOS is a single-pulse thermal switching [4, 5] that is not limited to Gd-based ferrimagnetic alloys but has also been observed in Gd-based ferrimagnetic multilayers [6, 7] and the ferrimagnetic Heusler alloy, Mn_2Ru_xGa [8]. However, AOS is also found to be helicity-dependent in some materials such as ferrimagnetic Tb-transition metal (TM) alloys [9], synthetic ferrimagnets [10, 11], and ferromagnetic Co/Pt multilayers [12]. It was initially thought that the circularly polarized light acted as an effective magnetic field, due to the inverse Faraday effect (IFE), in the spin system during helicity-dependent AOS (HD-AOS) [13–15]. The strength and lifetime of the induced field pulses remain an open question. When HD-AOS is studied in the ultrafast time domain [16], the effective magnetic field strength due to the IFE has to be as large as 10 T to achieve such a short switching time according to the theoretical simulations. A minimal IFE lifetime of 0.15 ps was estimated for Co/Pt [13], while longer durations of several picoseconds after the laser pulse excitation have also been reported [17–20]. Furthermore, the IFE response has been found to be strongly material dependent, and the interlayer exchange interactions and spin–orbit coupling are considered to play an essential role in HD-AOS of magnetic multilayers [21]. An optical spin-transfer torque was also suggested to play a role in HD-AOS of ferromagnetic thin films with a Pt capping layer [22]. Other mechanisms put forward to account for HD-AOS include laser-induced heating [23, 24], magnetic circular dichroism (MCD) [25, 26], and optical selection rule [27].

Heating and helicity effects are entangled in HD-AOS using circularly polarized laser pulses, and the individual contribution cannot be distinguished by using just one circularly polarized pump beam. Furthermore, as the HD-AOS has been reported as a multi-pulse effect [28], the important information, such as the onset and duration of helicity effects and interplay between the heating and helicity effects in the first few picoseconds of HD-AOS switching processes, cannot be obtained from a conventional time-resolved measurement with a single pump beam [12, 16, 20, 25]. This paper employed a dual-pumping scheme working with magneto-optical Kerr effect (MOKE) microscopy to investigate HD-AOS in a Pt/Co/Pt triple-layer sample, as shown schematically in Fig. 1a, to identify individual contributions from heating and helicity effects and distinguish the time dependence between them.

This dual-pumping scheme [17, 29] allows one to choose the helicity of each pump pulse independently and vary both the power combination and time delay between the two pump pulses. The transient pre-heated state of the electron-spin system, on which the second CP pump pulse is to impinge, can be tuned by controlling the power of the first linearly polarized (LP) pump pulse as well as the precise time delay between the two pulses, as indicated in Fig. 1b. HD-AOS can be achieved with circularly polarized laser pulses with very low fluences if a LP pulse is used to preheat the system into a reduced magnetization state. The strong correlation between HD-AOS and the time interval between the LP and CP pulses signposts an instant onset of helicity effect, but only lasting for a period of the order of the laser pulse duration. The pre-heated transient demagnetized state is found to play a key role in realizing HD-AOS.

2 Experimental

2.1 Sample fabrication

The sample used in this study was a Pt (2 nm)/Co (0.6 nm)/Pt (2 nm) triple-layer grown on a 5 nm Ta buffer layer. The film was deposited on a Corning glass substrate with a thickness of 0.13 mm at room temperature by direct-current (DC) magnetron sputtering. The base pressure of the sputtering system was better than 4×10^{-5} Pa. The Ar pressure during growth was 0.5 Pa. The sputtering rate with a DC of 40 mA was 0.041, 0.084 and 0.048 $nm \cdot s^{-1}$ for Ta, Pt and Co, respectively. The Ta buffer layer was employed to improve the Pt/Co interface smoothness and the (111) orientation and enhance the Co layer's perpendicular magnetic anisotropy. This is confirmed in the MOKE hysteresis loop shown in Fig. 2. Here Fig. 2a is measured by the MOKE image system used in the AOS experiments and Fig. 2b is measured by the vibrating-sample magnetometer (VSM). Both loops prove that the sample has a well-defined perpendicular magnetic anisotropy.

2.2 Experimental method

Figure 3 is a schematic diagram of the double pump experimental setup, a combination of time-resolved pump-probe and MOKE image systems. For the MOKE imaging system part, the light-emitting diode provides a 465 nm light to the system. The objective lens chosen in this experiment is HALO, and the numerical aperture (NA) is 0.38. Since such an objective and blue light were used for illumination, domains as narrow as 612 nm can be resolved. A Ti:sapphire laser amplifier system with 150 fs pulse duration, 800 nm central wavelength, and a 1000 Hz repetition rate was used. For the dual-pumping measurements, the pulse was split into two pulses. The first pump pulse was LP and used to heat the sample's electron/spin systems. The second pump pulse was circularly polarized (CP), delayed with respect to the first LP pulse, and used to switch the sample's magnetic state, as illustrated in Fig. 1a.

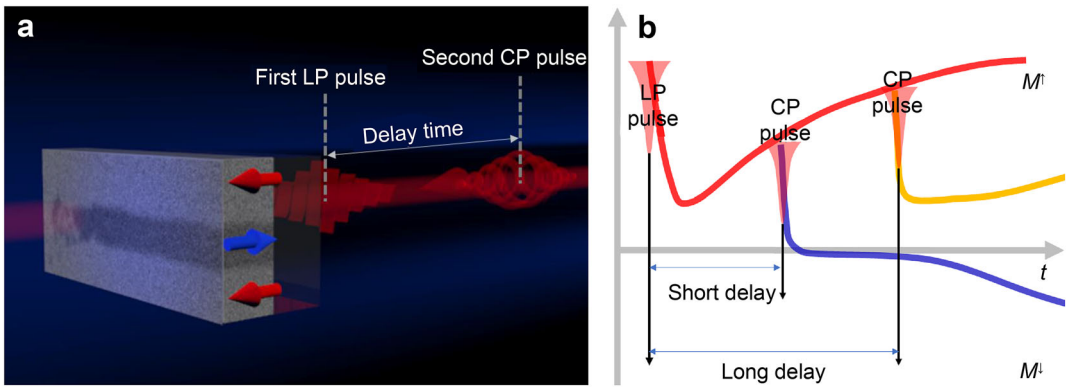

Fig. 1 Double-pump scheme and its implementation: **a** magnetic domain image of Pt/Co/Pt triple-layer sample under laser illumination from substrate side, where magnetization is initially saturated along perpendicular direction of sample plane labelled as $M^{\uparrow}$ state (red arrows), area exposed under laser is switched to opposite direction, labelled as $M^{\downarrow}$ state (blue arrow) **b** magnetization of exposed area as a function of time with dual-pulse excitation, where the first LP pulse heats sample to a demagnetized state (red curve), the second CP pulse arrives after a certain delay, for a short delay, domain switching is expected (blue curve), but for a long delay, switching may not occur (yellow curve)

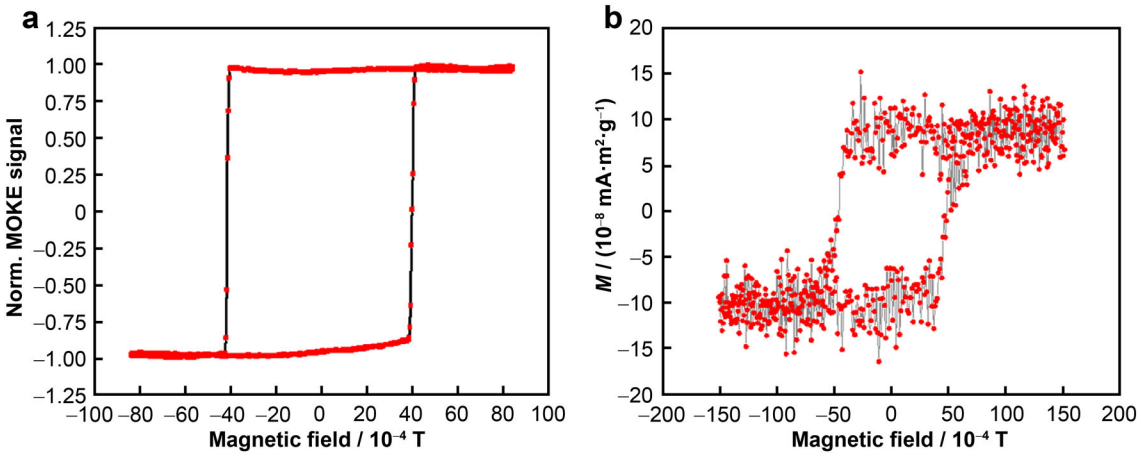

Fig. 2 Magnetic hysteresis loops of glass/Ta (5 nm)/Pt (2 nm)/Co (0.6 nm)/Pt (2 nm) sample at room temperature: **a** measured by MOKE image system; **b** measured by VSM

The power of each pump beam was individually adjusted for the desired power combination. The two pump beams were combined at a beam splitter before focusing onto the Pt/Co/Pt triple-layer from the substrate side. The spot size was measured as 38 μm in diameter using a charge-coupled device (CCD) beam profiler which gave a laser fluence of 8.83×10^{-2} mJ·cm^{-2} at an average laser power of 1μW. The sample was mounted on a motorized 3-axis nanomax flexure stage. The magnetization of the sample was initially saturated along the perpendicular direction of the sample plane, defined as $M^{\uparrow}$ state. When the sample was exposed to the dual-pump beams, the stage was scanned over a 300 μm distance at a velocity of 10 μm·s^{-1}. After laser excitation, the magnetic domain state was recorded as a MOKE image via wide-field MOKE microscopy. The sample was then re-magnetized to the $M^{\uparrow}$ state, and a reference MOKE image was taken. The MOKE images presented are the subtractions of each pair of these images, where most of the effects from the surface morphology are eliminated.

3 Results and discussion

3.1 Experimental results

HD-AOS induced by LP and CP pulse pairs with different power combinations at a fixed delay time, 1.6 ps, between them were investigated first. The energy transfer for the electron-spin system to the lattice system is mediated by the phonons, which takes about 1.6 ps to reach the spin-electron-lattice thermal equilibrium state [30–32] with the system in a largely demagnetized state when the second CP

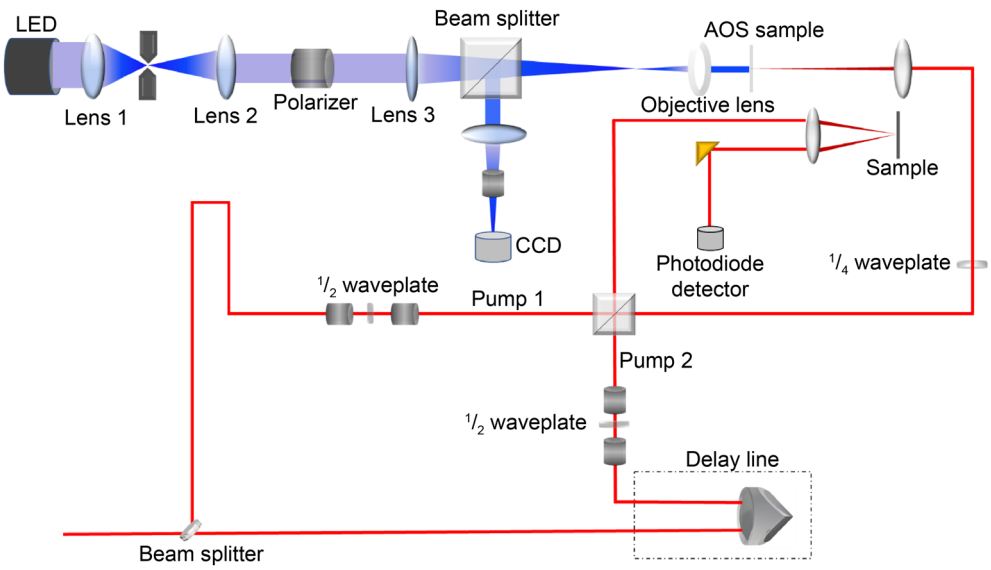

Fig. 3 Magneto-optical Kerr microscope coupled to time-resolved (TR)-MOKE laser system, where 465 nm light-emitting diode (LED) served as a light source for Kerr microscopy, reflected imaging beam was directed towards CCD camera by a polarizing beam splitter; as sample's substrate is glass, laser beam was focused by another objective lens and passed through sample from glass substrate side

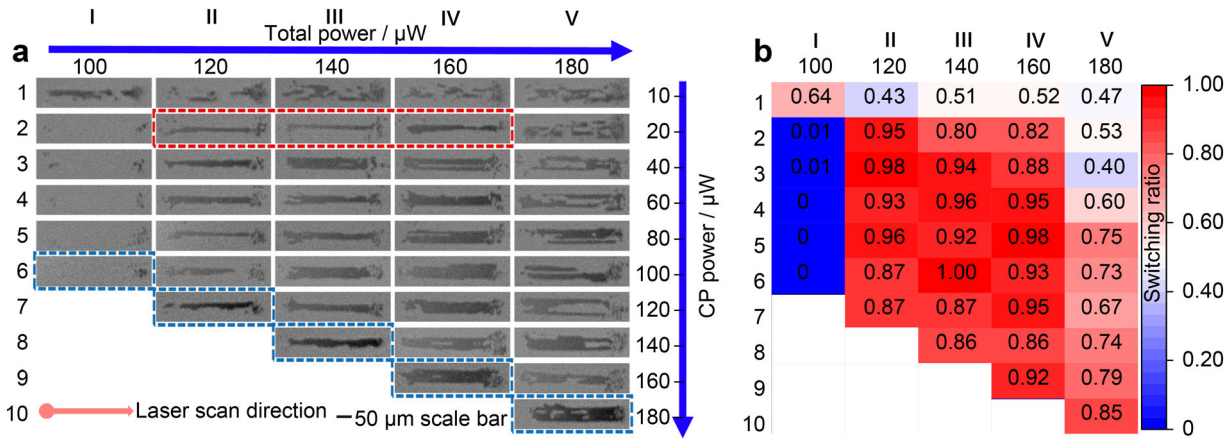

Fig. 4 HD-AOS induced by dual-pump with different power combinations at a fixed time interval: **a** MOKE images of magnetic domains induced by a sequence of LP and CP pulse pairs; **b** extracted switching ratio for each image frame

pulse arrives. Figure 4a shows each subtracted MOKE image centered along the scanning path of the dual-pump beam with a field of view of 60 μm × 380 μm. The horizontal axis shows the total power of the LP and CP pulse pairs increasing from 100 to 180 μW, while the vertical axis gives the power of the CP pulse increasing from 10 μW to the total power of each column. The power of the LP pulse used for each image is the difference between the total power and the CP pulse power. The MOKE images, framed in blue dashed lines, exhibit AOS with only CP pulses incident. The switching ratio is calculated by dividing the total number of switched pixels by the total number of pixels within a 20 μm × 200 μm window in each image of Fig. 4a, resulting in switching ratio mapping, as shown in Fig. 4b. In Fig. 4a, the images of the first-row show that a random domain state is generated by 10 μW beam power combined with various power preheat LP. The switching ratio range of each image in the first row is 43% to 64% (as shown in Fig. 4b), which indicates a multidomain state caused by the low power of CP.

Once the CP beam power is increased to 20 μW and beyond, HD-AOS is observed with a total power window of 120 μW(10.6 mJ·cm^{-2}) to 160 μW (14.1 mJ·cm^{-2}). The switching ratio is above 80% across this whole power window. It indicates that the power window for pairs of LP and CP pulses is the same as for a single CP pulse when the second CP arrives at a 1.6 ps time delay. In the column of the 160 μW total power, multidomain patterns can be seen

to emerge in the center of the laser beam path. When the total power is increased to 180 μW, the multidomain pattern is created regardless of beam power combinations. Even though the switching ratio is over 60% under the 180 μW total beam power induced, the laser causes irreversible changes in the sample's magnetic properties leading to increased coercivity of the exposed area. Therefore, 180 μW is excluded from the quoted power window of HD-AOS. The occurrence of the multidomain states under high power laser pumping is due to the laser heating the sample to sufficiently high levels to demagnetize the sample again after HD-AOS. As shown in the images framed in dashed red lines in Fig. 4a, the laser-swept area remains a uniformly switched magnetic domain even when the power of the CP beam is reduced to 20 μW with the samples preheated by the LP pulse. The corresponding switching ratios are all above 80%, as shown in Fig. 4b.

Therefore, the minimum power of the CP pulse required to achieve HD-AOS with LP preheated is 20 μW for our sample. When the sample is sufficiently demagnetized, circularly polarized illumination with a power threshold as low as 1.77 mJ·cm^{-2}, reduced by 80% compared to that without-preheating, is sufficient to achieve HD-AOS as demonstrated by the images framed in red dashed lines in Fig. 4a. This proves that laser heating plays an essential role in HD-AOS of the Pt/Co/Pt triple-layer, where only a single magnetic lattice exists, compared to HID-AOS in RE-FM alloy/multilayers [5, 6]. This discovery reveals that most of the required pulse energy is used to heat the spin system in a single-pump-induced HD-AOS event in the Pt/Co/Pt structure [21]. The helicity effect requires only a small portion of the power threshold.

As indicated in Fig. 1b, the delay time between the LP and CP on HD-AOS is a critical factor. To study this effect in detail, the delay time was set from 0 to 10 ps, with a step size of 0.2 ps for the first 2 ps and then 0.5 ps afterward. The CP beam power was increased from 20 to 100 μW with a step size of 10 μW, while the LP was decreased from 100 to 20 μW, so that the total power was fixed at 120 μW, which was the minimum total laser power needed for HD-AOS in the sample. The switching ratio of HD-AOS was extracted for each MOKE image captured at every delay time, quantified via image processing using ImageJ [33], and plotted as a function of time delay in Fig. S5 (see Supporting Information for details). The MOKE images and the extracted switching ratio of two representative power combinations are displayed in Fig. 5. The interference of the two pump pulses at the zero-delay point induced a multidomain state, which leads to an approximate 50% switching ratio for every curve in Fig. 5c, d at the zero-delay point. With the delay time increasing, the switching ratio increases first and reaches its highest point, approximately 90%, when the time delay is about 1 ps for all the power combinations. However, after the initial rise, the switching ratio significantly differs in its dependence on the LP and CP time delay between these two power combinations. For the case of LP power 40 μW (3.53mJ·cm^{-2}) and CP power 80 μW, the switching ratio drops sharply when the time delay between the two pulses is longer than 2 ps. It decreases to less than 20% when the time delay is longer than 3 ps, as shown in Fig. 5c. On the other hand, for the case of LP power 80 μW (7.06mJ·cm^{-2}) and CP power 40 μW, the switching ratio stays at its highest value ($\sim$ 90%) for the time delay from 1 to 4 ps. When the time delay is longer than 4 ps, the switching ratio drops very slowly and gradually to around 60% up to 300 ps. When the time delay is longer than 300 ps, the switching rate drops dramatically below 50%, as shown in Fig. 5d. The gradual decrease in the switching rate between 4 and 300 ps delay is large due to the shrinking of the switching area. As shown in Fig. 5b, the width of the central black trace decreased with the delay time increase while the switching rate was calculated within a window of fixed size of 20 μm × 200 μm. These two different processes are also evidenced in their MOKE images at different time delays, as presented in Fig. 5a and b. In Fig. 5a, for the case of LP power of 40 μW, there is no sign of switching at 6 ps, while Fig. 5b shows a clear switching at the same delay time, but with a larger LP power of 80 μW.

Atomistic spin dynamics modelling combined with a two-temperature model has been employed to simulate the demagnetization rate and magnetization recovery after the LP pulse for both cases, i.e., of 40 and 80 μW, and the results are superimposed on their switching rate curves in Fig. 5c and d, respectively. To simplify the analysis, we consider the spin system is coupled to the temperature profile of the electrons in the two-temperature model. It shows that the magnetization recovery (spin cooling) time after laser excitation increases from a couple of picoseconds to a few hundreds of picoseconds as the LP power increases from 40 to 80 μW, which was also observed in the time-resolved MOKE measurements of the sample shown in Fig. S6. A red dotted horizontal line is drawn at the 50% switching ratio (left-hand *y*-axis) in both Fig. 5c and d. In Fig. 5c, HD-AOS occurs when the 80 μW CP pulse arrives within a time delay between 0.2 and 2 ps, shaded in grey. In Fig. 5d, HD-AOS occurs when the 40 μW CP pulse arrives within a time delay from 0.2 to over 300 ps, also shaded in grey. Comparing the sample magnetic states within these two grey areas where HD-AOS is achieved, one can see a common minimum of the sample magnetization of around 60% of the saturation magnetization. This indicates that the demagnetized state upon which the CP pulse impinges is a key factor in achieving HD-AOS.

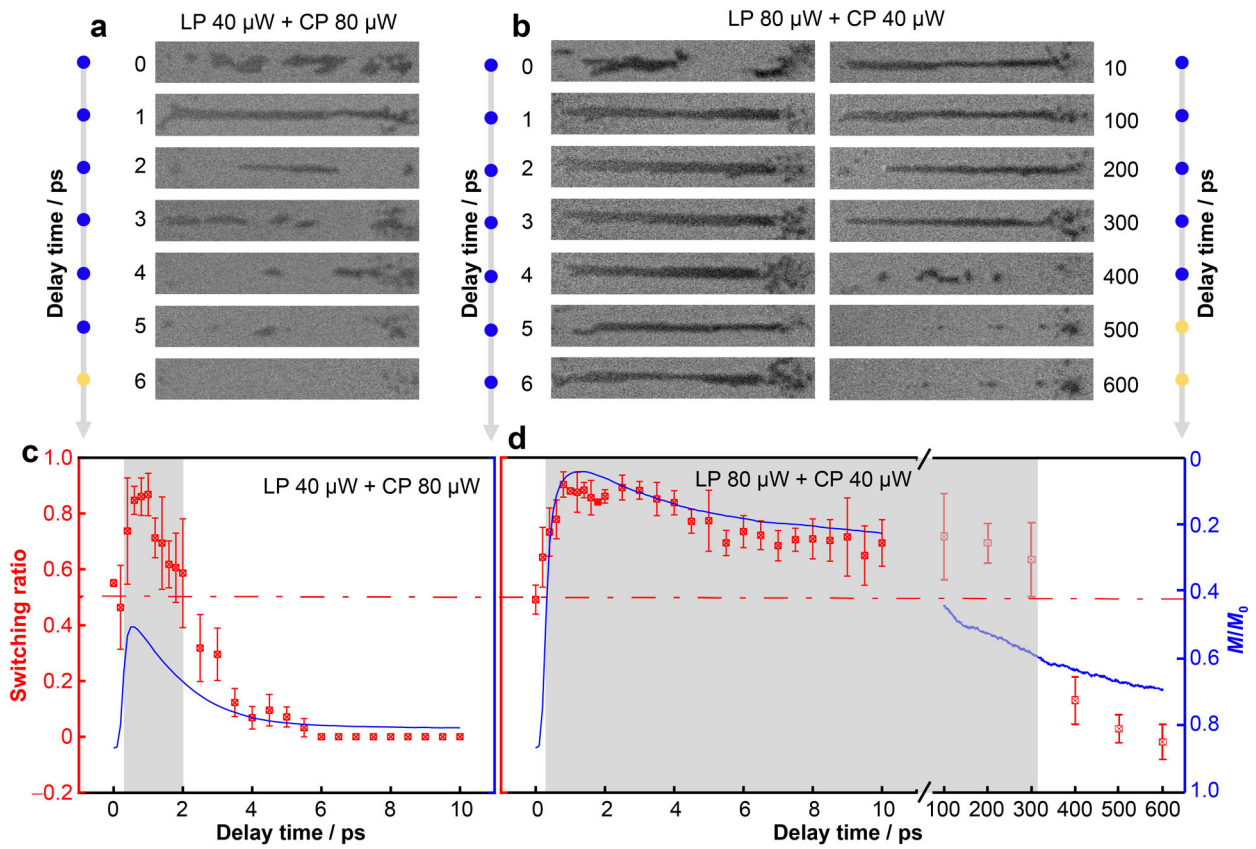

Fig. 5 HD-AOS as a function of time interval between two pulses: MOKE images of magnetic domains induced under two different combinations of LP and CP powers: **a** LP 40 μW + CP 80 μW and **b** LP 80 μW + CP 40 μW (number next to each image indicating delay time); switching ratio vs. delay time and simulated demagnetization curves of magnetic domains induced under two different combinations of LP and CP powers: **c** LP 40 μW + CP 80 μW and **d** LP 80 μW + CP 40 μW (horizontal red-dotted lines indicating a switching ratio of 50%)

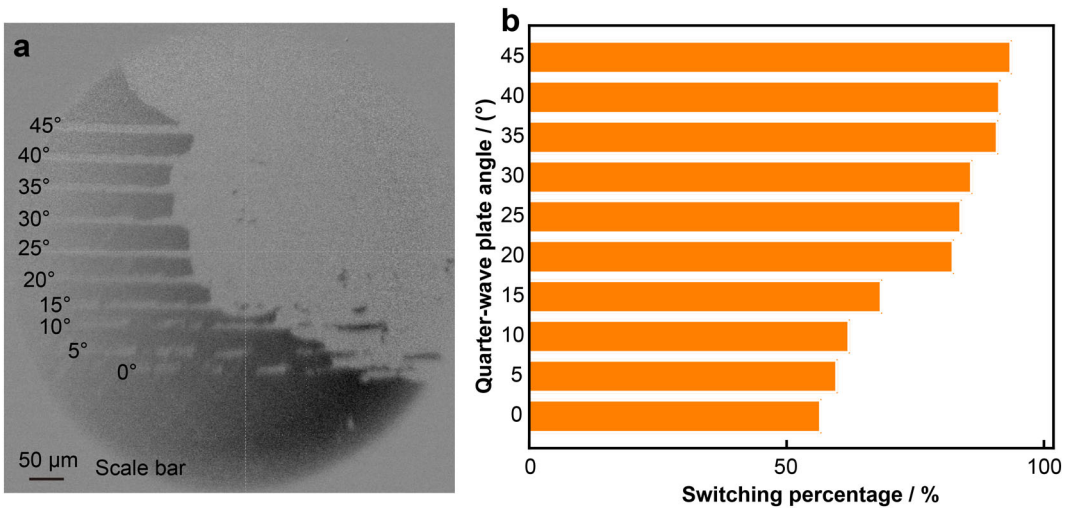

Fig. 6 **a** Magneto-optical Kerr image of all optical switching in a Pt(2 nm)/Co(0.6 nm)/Pt(2 nm) thin film exposed to 120 μW RCP laser with different light ellipticity which is changed by rotating angle of quart-wave plate as labelled on left; **b** corresponding AOS switching ratio of **a**

The relationship between HD-AOS switching ratio and laser ellipticity was further investigated by using a single pump, and the results are included in Fig. 6. The light ellipticity is tuned by the quarter-wave plate and the number on the left of Fig. 6a indicates the quarter wave plate's angle. Here 45° gives the right-handed circularly polarized (RCP) light, and 0° gives the LP light. The laser power is fixed at 120 μW in this experiment. The elliptically polarized light can be regarded as a combination of LP and CP. The switching ratio was found to decrease as the laser polarization changed from circular to linear. This is consistent with a previous finding on laser-induced domain wall motion, where wall displacement decreases as laser polarization changes from circular to linear [16]. For these single pulse cases, the LP and CP photons arrived simultaneously, and the heating effect from the LP photons lags; thus, the CP photons fail to achieve HD-AOS. This can account for the fact that HD-AOS has not been observed in a wider range of material systems because, generally, ultrafast laser heating effects lag behind its helicity effect. This also explains a previous observation that a longer laser pulse duration gives a higher switching ratio under the same laser power AOS [34]. As shown in Fig. S6, the higher laser fluence takes longer to reach the highest demagnetized state as pointed out previously [35]. With the dual-pump laser pulses, we expect that HD-AOS would occur in many other magnetic materials where the transient magnetization states needed for the CP lighted driven HD-AOS can be achieved by controlling the strength of the LP pulse and the delay time.

3.2 Discussion

The essential role of heating in HD-AOS alone cannot explain the dramatically different time-delay dependence between the above two cases since the second CP pulse also heats the sample, which reduces the magnetization. As shown in Fig. 7a, the first LP pulse increases both $M^{\uparrow}$ and $M^{\downarrow}$ domains' temperature but not close to the Curie temperature (T_c). While due to the MCD effect, the second CP pulse heats the $M^{\uparrow}$ domain's temperature closer to T_c. Once it switched to $M^{\downarrow}$ domain, it absorbs fewer CP photons and makes its temperature away from T_c. However, this phenomenological mechanism should not be sensitive to the time sequence of the CP and LP pulses. As shown in Fig. 7b, if the CP pulse arrived first, it still gives a temperature difference of $T_1^{\uparrow}$ and$T_1^{\downarrow}$. And then, the second LP pulse increases both domains' temperature but keeps the temperature difference. Then the HD-AOS still can happen. Also, in Fig. 7c, the elliptically polarized pulse can be regarded as a mixture of CP and LP pulses. Based on the MCD effect, it still induces a temperature difference between $M^{\uparrow}$ and $M^{\downarrow}$ domains. However, the 60 μW LP + 60 μw CP (LP arrived first) gives the same AOS ratio as the 120 μW CP pulse, but if they arrived simultaneously (elliptically polarized pulse), the switching ratio is lower than the formers. In contrast, the AOS is not observed if the CP pulse arrived earlier than the LP pulse. Moreover, in our double pump experiments (especially the 100 μW LP + 20 μW CP), the temperature difference between these two domains is much smaller than using a single 120 μW CP pump, while these two experiments give a nearly same switching ratio. Here, the spin heat capacity (C_s) change with the spin system's temperature (T_s) was not considered. MCD is introduced to explain the laser-induced domain wall motion [16]. We would like to emphasize that several more effects should be considered to fully explain our results based on the MCD mechanism.

To clarify this picture, atomistic spin dynamics modelling combined with a two-temperature model has been applied again to simulate the demagnetization rate and magnetization recovering excited by both the LP and CP pulses. Figure 8a and b shows the case when two pulses are 5 ps apart. A red dashed horizontal line is drawn at 60% of

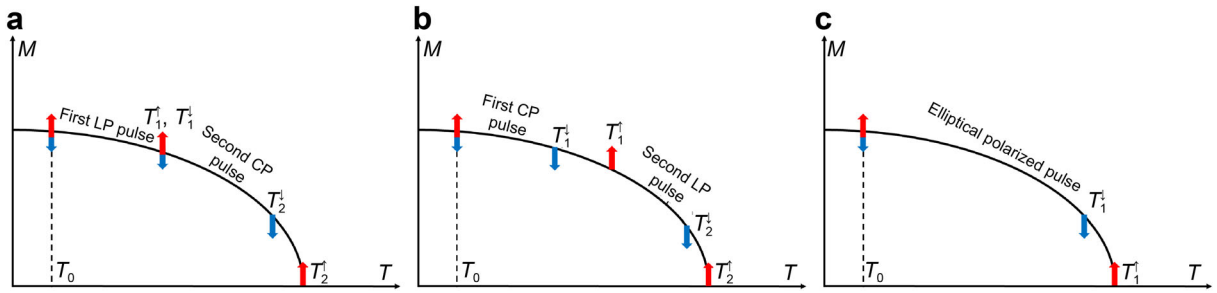

Fig. 7 HD-AOS model based on MCD mechanism: **a** LP pulse arriving first, and then CP pulses; **b** CP pulse arriving first, and then LP pulse; **c** using elliptically polarized pulse. Here, the horizontal axis shows the temperature of the magnetic domain, and the vertical axis gives the magnetization. $T_{1(2)}^{\uparrow(\downarrow)}$ presents the temperature of the magnetic domain with spin up (down) after excited by the first (second) laser pulse

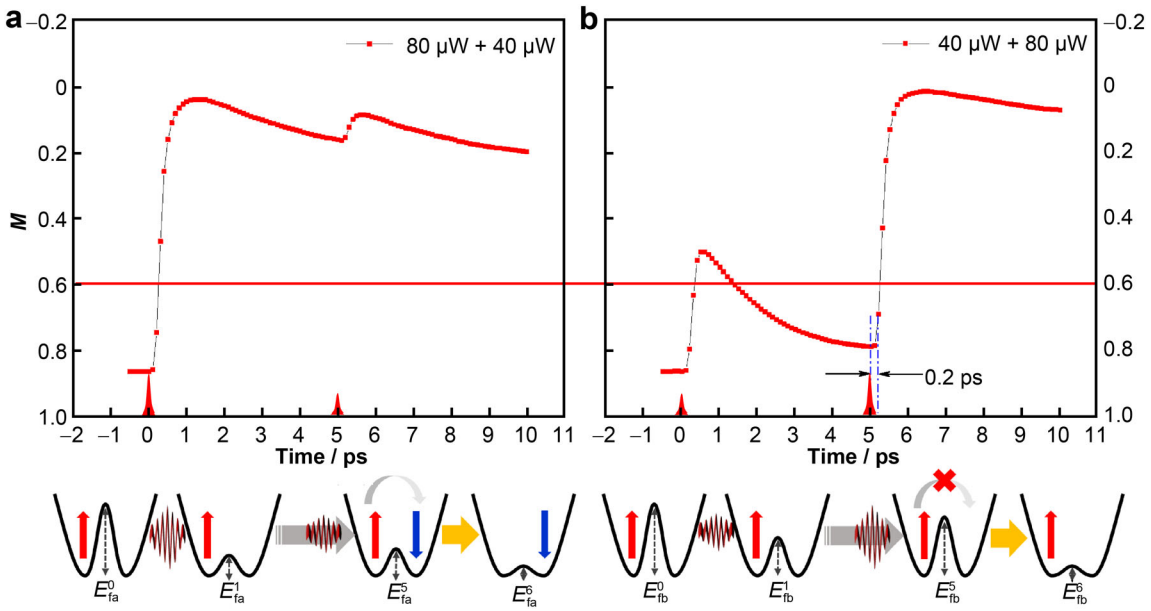

Fig. 8 Simulation of dual-pump induced magnetic switching process: **a** LP 80 μW + CP 40 μW and **b** LP 40 μW + CP 80 μW (two short vertical dashed lines (blue) in **b** marking 0.2 ps time intervals after CP pulse excitation; effective energy barriers (E^t_{fa}, E^t_{fb}), determined by transient spin temperatures, between $M^{\uparrow}$ states and $M^{\downarrow}$ states at four-time delays (t, ps) being illustrated for both cases)

the saturation magnetization value in Fig. 8, which is the maximum magnetization observed in the two grey areas in Fig. 5. The spin-flip energy barriers related to the spin temperatures are also added and represented by E^t_{fa} and E^t_{fb}, respectively, where t represents the delay time. To identify the lag between the helicity and heating effects, we show the corresponding E^t_f at four-time points, namely when: the first pulse arrival time ($t = 0$), the first demagnetization peak occurs ($t = 1$ ps), the second pulse arrival time ($t = 5$ ps), and when the second demagnetization peak occurs ($t = 6$ ps). It can be seen that in the case of Fig. 8a with the LP 80 μW + CP 40 μW pulse combination, at 5 ps delay time, the sample's magnetization has only recovered 20%. This corresponds to a lower energy barrier E^5_{fb} between $M^{\uparrow}$ and $M^{\downarrow}$ states upon the arrival of the 40 μW CP pulse, and HD-AOS takes place in this case. In the case of Fig. 8b with LP 40 μW+ CP 80 μW pulse pair, at 5 ps delay time, the sample magnetization recovers to around 80% of its saturation value. This corresponds to a high energy barrier E^5_{fa} between $M^{\uparrow}$ and $M^{\downarrow}$ states upon the arrival of the 80 μW CP pulse, and HD-AOS doesn't take place. This is because the CP pulse's heating effect takes more than 0.3 ps to demagnetize the sample's magnetization to its second peak. During the CP pulse duration, the sample's magnetization is only reduced to 70% of its saturation value, as marked by two short vertical dash lines in Fig. 8b. The only explanation for this observation is that the onset time of the helicity effect from the CP pulse is instant, and the duration of the helicity effect is less than 200 fs which is close to the laser pulse width of 150 fs. Even though the energy barrier E^6_{fb} is reduced further by the heating effect of the CP pulse itself, the helicity effect has already disappeared at this point, and HD-AOS cannot be triggered anymore.

4 Conclusion

In conclusion, the dual-pulse laser excitation method was applied to identify the contribution and time dependence of the heating and helicity effects on HD-AOS in a Pt/Co/Pt triple-layer. The results show that pre-heating plays an essential role in HD-AOS. The laser power required for HD-AOS via the helicity effect was reduced by 80% when the magnetization is close to a fully demagnetized state. By varying the time delay between LP and CP pulses with different energy combinations, it can be demonstrated unambiguously that the helicity effect which gives rise to the deterministic helicity-induced switching, occurs instantly within 200 fs upon laser excitation, close to the laser pulse duration. This work reveals heating and helicity effects' timescales in helicity-dependent all-optical magnetization switching. At the same time, the unique LP/CP dual-pump scheme makes the manipulation of HD-AOS feasible, which provides a promising way for achieving HD-AOS in a wide range of material systems [36, 37].

Acknowledgements This work is financially supported by the National Key Research and Development Program of China (No. 2016YFA0300803), the National Natural Science Foundation of China (Nos. 61427812 and 11774160), the Natural Science

Foundation of Jiangsu Province of China (No. BK20192006). X. Lu acknowledges the support of National Key R&D Program of China (No. 2021YFB3601600) and the Natural Science Foundation of Jiangsu Province of China (No. BK20200307). T. A. Ostler gratefully acknowledges the support of the UK EPSRC (No. EP/T027916/1). This work was supported by the EPSRC TERASWITCH project (project ID EP/T027916/1)

Declarations

Conflict of interests The authors declare that they have no conflict of interest.

References

[1] Stanciu CD, Hansteen F, Kimel AV, Kirilyuk A, Tsukamoto A, Itoh A, Rasing T. All-optical magnetic recording with circularly polarized light. Phys Rev Lett. 2007;99(4):47601. https://doi.org/10.1103/PhysRevLett.99.047601.

[2] Ostler TA, Barker J, Evans RF, Chantrell RW, Atxitia U, Chubykalo-Fesenko O, El Moussaoui S, Le Guyader L, Mengotti E, Heyderman LJ, Nolting F, Tsukamoto A, Itoh A, Afanasiev D, Ivanov BA, Kalashnikova AM, Vahaplar K, Mentink J, Kirilyuk A, Rasing T, Kimel AV. Ultrafast heating as a sufficient stimulus for magnetization reversal in a ferrimagnet. Nat Commun. 2012;3:666. https://doi.org/10.1038/ncomms1666.

[3] Radu I, Vahaplar K, Stamm C, Kachel T, Pontius N, Durr HA, Ostler TA, Barker J, Evans RF, Chantrell RW, Tsukamoto A, Itoh A, Kirilyuk A, Rasing T, Kimel AV. Transient ferromagnetic-like state mediating ultrafast reversal of antiferromagnetically coupled spins. Nature. 2011;472(7342):205. https://doi.org/10.1038/nature09901.

[4] Atxitia U, Ostler TA. Ultrafast double magnetization switching in GdFeCo with two picosecond-delayed femtosecond pump pulses. Appl Phys Lett. 2018;113(6):062402. https://doi.org/10.1063/1.5044272.

[5] Yang Y, Wilson RB, Gorchon J, Lambert CH, Salahuddin S, Bokor J. Ultrafast magnetization reversal by picosecond electrical pulses. Sci Adv. 2017;3(11): e1603117. https://doi.org/10.1126/sciadv.1603117.

[6] Lalieu MLM, Peeters MJG, Haenen SRR, Lavrijsen R, Koopmans B. Deterministic all-optical switching of synthetic ferrimagnets using single femtosecond laser pulses. Phys Rev B. 2017;96(22):220411. https://doi.org/10.1103/PhysRevB.96.220411.

[7] Remy Q, Igarashi J, Iihama S, Malinowski G, Hehn M, Gorchon J, Hohlfeld J, Fukami S, Ohno H, Mangin S. Energy efficient control of ultrafast spin current to induce single femtosecond pulse switching of a ferromagnet. Adv Sci (Weinh). 2020;7(23):2001996. https://doi.org/10.1002/advs.202001996.

[8] Banerjee C, Teichert N, Siewierska KE, Gercsi Z, Atcheson GYP, Stamenov P, Rode K, Coey JMD, Besbas J. Single pulse all-optical toggle switching of magnetization without gadolinium in the ferrimagnet Mn_2Ru_xGa. Nat Commun. 2020;11(1):4444. https://doi.org/10.1038/s41467-020-18340-9.

[9] Lu XY, Zou X, Hinzke D, Liu T, Wang YC, Cheng TY, Wu J, Ostler TA, Cai JW, Nowak U, Chantrell RW, Zhai Y, Xu YB. Roles of heating and helicity in ultrafast all-optical magnetization switching in TbFeCo. Appl Phys Lett. 2018;113(3):3425. https://doi.org/10.1063/1.5036720.

[10] Mangin S, Gottwald M, Lambert CH, Steil D, Uhlir V, Pang L, Hehn M, Alebrand S, Cinchetti M, Malinowski G, Fainman Y, Aeschlimann M, Fullerton EE. Engineered materials for all-optical helicity-dependent magnetic switching. Nat Mater. 2014;13(3):286. https://doi.org/10.1038/nmat3864.

[11] Liao JW, Vallobra P, O'Brien L, Atxitia U, Raposo V, Petit D, Vemulkar T, Malinowski G, Hehn M, Martinez E, Mangin S, Cowburn RP. Controlling all-optical helicity-dependent switching in engineered rare-earth free synthetic ferrimagnets. Adv Sci (Weinh). 2019;6(24):1901876. https://doi.org/10.1002/advs.201901876.

[12] Lambert CH, Mangin S, Varaprasad BS, Takahashi YK, Hehn M, Cinchetti M, Malinowski G, Hono K, Fainman Y, Aeschlimann M, Fullerton EE. All-optical control of ferromagnetic thin films and nanostructures. Science. 2014;345(6202):1337. https://doi.org/10.1126/science.1253493.

[13] Cornelissen TD, Cordoba R, Koopmans B. Microscopic model for all optical switching in ferromagnets. Appl Phys Lett. 2016;108(14):14208. https://doi.org/10.1063/1.4945660.

[14] Berritta M, Mondal R, Carva K, Oppeneer PM. Ab initio theory of coherent laser-induced magnetization in metals.Phys Rev Lett. 2016;117(13):137203. https://doi.org/10.1103/PhysRevLett.117.137203.

[15] Popova D, Bringer A, Blugel S. Theoretical investigation of the inverse Faraday effect via a stimulated Raman scattering process. Phys Rev B. 2012;85(9):0944191. https://doi.org/10.1103/PhysRevB.85.094419

[16] Quessab Y, Medapalli R, El Hadri MS, Hehn M, Malinowski G, Fullerton EE, Mangin S. Helicity-dependent all-optical domain wall motion in ferromagnetic thin films. Phys Rev B. 2018;97(5):054419. https://doi.org/10.1103/PhysRevB.97.054419.

[17] Alebrand S, Hassdenteufel A, Steil D, Cinchetti M, Aeschlimann M. Interplay of heating and helicity in all-optical magnetization switching. Phys Rev B. 2012. https://doi.org/10.1103/PhysRevB.85.092401.

[18] Kimel AV, Kirilyuk A, Usachev PA, Pisarev RV, Balbashov AM, Rasing T. Ultrafast non-thermal control of magnetization by instantaneous photomagnetic pulses. Nature. 2005;435(7042):51. https://doi.org/10.1038/nature03564

[19] Vahaplar K, Kalashnikova AM, Kimel AV, Hinzke D, Nowak U, Chantrell R, Tsukamoto A, Itoh A, Kirilyuk A, Rasing T. Ultrafast path for optical magnetization reversal via a strongly nonequilibrium state. Phys Rev Lett. 2009. https://doi.org/10.1103/PhysRevLett.103.117201.

[20] Nieves P, Chubykalo-Fesenko O. Modeling of ultrafast heat- and field-assisted magnetization dynamics in FePt. Phys Rev Appl. 2016. https://doi.org/10.1103/PhysRevApplied.5.014006.

[21] Hellman F, Hoffmann A, Tserkovnyak Y, Beach GSD, Fullerton EE, Leighton C, MacDonald AH, Ralph DC, Arena DA, Durr HA, Fischer P, Grollier J, Heremans JP, Jungwirth T, Kimel AV, Koopmans B, Krivorotov IN, May SJ, Petford-Long AK, Ron-

dinelli JM, Samarth N, Schuller IK, Slavin AN, Stiles MD, Tchernyshyov O, Thiaville A, Zink BL. Interface-induced phenomena in magnetism. Rev Mod Phys. 2017. https://doi.org/10.1103/RevModPhys.89.025006.

[22] Choi GM, Schleife A, Cahill DG. Optical-helicity-driven magnetization dynamics in metallic ferromagnets. Nat Commun. 2017. https://doi.org/10.1038/ncomms15085.

[23] Moreno R, Ostler TA, Chantrell RW, Chubykalo-Fesenko O. Conditions for thermally induced all-optical switching in ferrimagnetic alloys: modeling of TbCo. Phys Rev B. 2017. https://doi.org/10.1103/PhysRevB.96.014409.

[24] Hoveyda F, Hohenstein E, Smadici S. Heat accumulation and all-optical switching by domain wall motion in Co/Pd superlattices. J Phys Condens Matter. 2017;29(22):22581. https://doi.org/10.1088/1361-648X/aa6c93.

[25] Gorchon J, Yang Y, Bokor J. Model for multishot all-thermal all-optical switching in ferromagnets. Phys Rev B. 2016. https://doi.org/10.1103/PhysRevB.94.020409.

[26] Khorsand AR, Savoini M, Kirilyuk A, Kimel AV, Tsukamoto A, Itoh A, Rasing T. Role of magnetic circular dichroism in all-optical magnetic recording. Phys Rev Lett. 2012. https://doi.org/10.1103/PhysRevLett.108.127205.

[27] Zhang GP, Babyak Z, Xue Y, Bai YH, George TF. First-principles and model simulation of all-optical spin reversal. Phys Rev B. 2017. https://doi.org/10.1103/PhysRevB.96.134407.

[28] Parlak U, Adam R, Burgler DE, Gang S, Schneider CM. Optically induced magnetization reversal in [Co/Pt](N) multilayers: role of domain wall dynamics. Phys Rev B. 2018. https://doi.org/10.1103/PhysRevB.98.214443.

[29] Yamada KT, Prabhakara KH, Li T, Ando F, Semin S, Ono T, Kirilyuk A, Kimel AV, Rasing T. Efficient all-optical helicity-dependent switching in Pt/Co/Pt with dual laser pulses. arXiv preprint arXiv:1903.01941, 2019.

[30] Chimata R, Bergman A, Bergqvist L, Sanyal B, Eriksson O. Microscopic model for ultrafast remagnetization dynamics. Phys Rev Lett. 2012. https://doi.org/10.1103/PhysRevLett.109.157201.

[31] Koopmans B, Malinowski G, Dalla Longa F, Steiauf D, Fahnle M, Roth T, Cinchetti M, Aeschlimann M. Explaining the paradoxical diversity of ultrafast laser-induced demagnetization. Nat Mater. 2010. https://doi.org/10.1038/nmat2593.

[32] Cheng TY, Wu J, Liu T, Zou X, Cai JW, Chantrell RW, Xu YB. Dual-pump manipulation of ultrafast demagnetization in TbFeCo. Phys Rev B. 2016. https://doi.org/10.1103/PhysRevB.93.064401.

[33] Schneider CA, Rasband WS, Eliceiri KW. NIH image to image J: 25 years of image analysis. Nat Methods. 2012. https://doi.org/10.1038/nmeth.2089.

[34] Medapalli R, Afanasiev D, Kim D, Quessab Y, Manna S, Montoya S, Kirilyuk A, Rasing T, Kimel A, Fullerton E. Multiscale dynamics of helicity-dependent all-optical magnetization reversal in ferromagnetic Co/Pt multilayers. Phys Rev B. 2017. https://doi.org/10.1103/PhysRevB.96.224421.

[35] Zhang W, He W, Peng LC, Zhang Y, Cai JW, Evans RFL, Zhang XQ, Cheng ZH. The indispensable role of the transversal spin fluctuations mechanism in laser-induced demagnetization of Co/Pt multilayers with nanoscale magnetic domains. Nanotechnology. 2018;29(27):275. https://doi.org/10.1088/1361-6528/aabdc9.

[36] Wang C, Zhu MG. Overview of composition and technique process study on 2:17-type Sm–Co high-temperature permanent magnet. Rare Met. 2020;40(4):790. https://doi.org/10.1007/s12598-020-01514-1.

[37] Weng XJ, Zhao GP, Tang H, Shen LC, Xiao Y. Thickness-dependent coercivity mechanism and hysteresis loops in hard/soft magnets. Rare Met. 2020;39(1):22. https://doi.org/10.1007/s12598-019-01264-9.